PERGAMON

International Journal of Solids and Structures 40 (2003) 5901–5921

INTERNATIONAL JOURNAL OF SOLIDS and STRUCTURES

www.elsevier.com/locate/ijsolstr

Three-dimensional solution of smart laminated anisotropic circular cylindrical shells with imperfect bonding

X. Wang *, Z. Zhong

Key Laboratory of Solid Mechanics of MOE, Department of Engineering Mechanics and Technology, Tongji University, Siping Road, Shanghai 200092, PR China

Received 19 February 2003; received in revised form 16 June 2003

Abstract

This paper presents an exact solution for a simply-supported and laminated anisotropic cylindrical shell strip with imperfect bonding at the off-axis elastic layer interfaces and with attached anisotropic piezoelectric actuator and sensor subjected to transverse loading. In this research, the imperfect interface conditions are described in terms of linear relations between the interface tractions in the normal and tangential directions, and the respective discontinuities in displacements. The solution for an elastic (or piezoelectric) layer of the smart laminated cylindrical shell strip is obtained in terms of the six-dimensional (or eight-dimensional) pseudo-Stroh formalism, solution for multilayered system is then derived based on the transfer matrix method. Finally, a numerical example is presented to demonstrate the effect of imperfect interface on the static response of the smart laminated cylindrical shell. The derived solutions can serve as benchmark results to assess various approximate shell theories and numerical methods.

Keywords: Composites; Anisotropic; Piezoelectric; Cylindrical shell; Layer; Imperfect interface; Pseudo-Stroh formalism; Transfer matrix

1. Introduction

Smart/intelligent materials and structures refer to structures with surface-mounted or embedded sensors and actuators. Laminated composites are well known for their high stiffness, strength and light-weight. Consequently, they can be used as load bearing part of the smart system. On the other hand, due to the direct piezoelectric effect and the inverse piezoelectric effect, piezoelectric materials can be employed as the sensing and actuating part of the smart system. A laminated anisotropic cylindrical shell with mounted anisotropic piezoelectric sensor and actuator is the focus of this research. Chen et al. (1997) considered a similar problem in a previous paper, but their solution is confined to shells with orthotropic piezoelectric and elastic layups. In this regard, this research can be considered as an extension of their results to the more general anisotropic cases.

* Corresponding author. Tel.: +86-653-63236; fax: +86-653-61015.
E-mail address: wjq_wang@sina.com (X. Wang).

0020-7683/$ - see front matter © 2003 Elsevier Ltd. All rights reserved.
doi:10.1016/S0020-7683(03)00389-5

In the mechanics of composite materials, it has been recognized that imperfect interfacial bonding has a significant influence on the behavior of fibrous composites (Achenbach and Zhu, 1990; Zhong and Meguid, 1997; Wang and Meguid, 1999; Tong et al., 2001; Liu et al., 2001; Wang and Shen, 2002). The presence of imperfectly bonded interfaces is also a common feature in many layered material systems such as delamination in laminated composites (Liu et al., 1994; Cheng et al., 1996; Tullini et al., 1998; Librescu and Schmidt, 2001) and slipping in asphalt pavements (Yue and Yin, 1998). Previous studies on the elastic behaviors of laminated composite shells, however, usually adopt a perfect interface model in which both displacements and tractions are continuous across each interface of dissimilar layers (Ren, 1987; Bhaskar and Varadan, 1993; Chen et al., 1997). Recently, various approximate two-dimensional theories of laminated composite shells have been proposed to incorporate the effect of damage due to the imperfect bonding between the constituent laminae (see for example, Cheng and Kitipornchai, 1998; Schmidt and Librescu, 1999; Librescu and Schmidt, 2001). There exist two restrictions in the theory of Cheng and Kitipornchai (1998). One restriction is that only a small amount of interfacial weakness is allowed because certain approximations have been made concerning displacement variation. The other one is that it is impossible to study the case of separation delamination by their theory because of neglect of transverse normal stress. The theory developed by Librescu and Schmidt (2001) concurrently incorporates the effects of imperfectly bonded interfaces, the effects of transverse shear and transverse normal strain, the dynamic effects, as well as the anisotropy of constituent material layers. Due to its general character, their theory can contribute to a more reliable prediction in the linear range of the load carrying capacity and failure of laminated composite shell structures featuring imperfectly bonded interfaces.

In this research, an exact three-dimensional electroelastic solution is obtained for cylindrical bending of simply-supported, infinitely long, transversely loaded laminated anisotropic cylindrical shell strips with imperfect bonding and with anisotropic piezoelectric layers acting as sensor and actuator. Here the imperfectly bonded interface formed by two adjacent elastic layers is modeled in terms of the linear springs. In this model of an imperfectly bonded interface, tractions are continuous but displacements are discontinuous across the interface. Furthermore, displacement jumps are proportional, in terms of the 'spring-factor-type' interface parameters, to their respective traction components. The solution for a homogeneous elastic (or piezoelectric) cylindrical shell is obtained in terms of the six-dimensional (or eight-dimensional) pseudo-Stroh formalism (Pan, 2001), solution for the smart multilayered cylindrical shell is derived based on the transfer matrix method (Yue and Yin, 1998; Pan, 2001). In the solution of Bhaskar and Varadan (1993) for an N-layered cylindrical shell, the $6N$ boundary and interface conditions yield a system of $6N$ algebraic equations to determine the $6N$ unknown coefficients. Consequently, their method is not suitable for addressing a cylindrical shell with very large number of layers (say, up to a hundred layers). This problem also exists in the solution of Chen et al. (1997). In the transfer matrix method adopted in this paper, however, the unknowns are the three displacements at the outer surface of the top piezoelectric actuator of the smart laminated shell and the three displacements at the inner surface of the bottom piezoelectric sensor of the smart laminated shell. By solving a system of six simultaneous linear equations, the six unknowns can be expressed in terms of the normal traction and electric potential applied on the outer surface of the top piezoelectric actuator. Consequently, the transfer matrix method is appropriate to treat a smart laminated shell with arbitrary number of layers.

2. Elastostatics of laminated shell

2.1. The boundary value problem

As illustrated in Fig. 1, the infinitely long and laminated shell panel considered here is composed of two anisotropic piezoelectric layers as its top and bottom layers and N dissimilar anisotropic elastic layers which

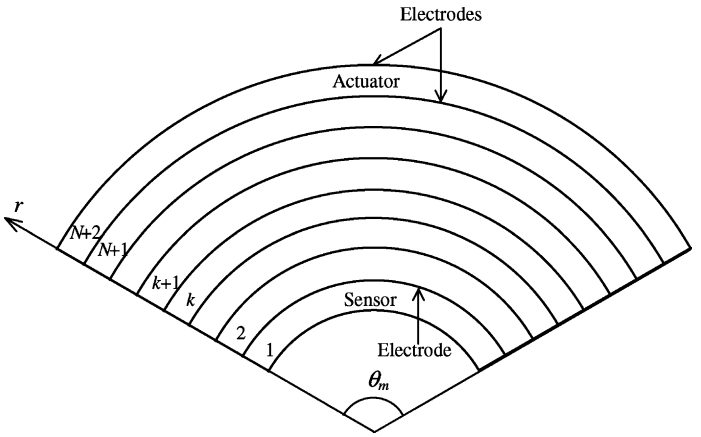

Fig. 1. Geometry of the smart laminated shell cross-section.

are imperfectly bonded. A cylindrical polar coordinate system (r, θ, z) is used, the jth $(1 \leqslant j \leqslant N+2)$ layer is bonded by the inner surface $r = R_{j-1}$ and the outer surface $r = R_j$, and the layers are numbered sequentially starting from the innermost layer. More specifically, each piezoelectric or elastic layer features cylindrical orthotropy, with its orthotropy axes not necessarily coinciding with the θ and z directions. The shell is in a state of generalized plane strain, i.e., displacements, electric potential, stresses and electric displacements are only functions of coordinates r and θ. In addition, the top piezoelectric layer is used as an actuator, while the bottom piezoelectric layer acts as a sensor. Two thin-film conducting electrodes are placed, respectively, on the two surfaces of the actuator to carry an alternating forcing electric potential, while one thin-film conducting electrode is placed on the outer surface of the sensor. For simplicity, the thickness of the electrode is ignored. The layered solid is subjected to a normal traction $q(\theta)$ and an electric potential $V(\theta)$, applied on the outer surface of the piezoelectric actuator, which can be assumed, without losing generality, as

$$q(\theta) = q_0 \sin(p\theta), \quad V(\theta) = V_1 \sin(p\theta), \quad p = m\pi/\theta_m, \tag{1}$$

where m is the number of the half-waves in the θ direction, and θ_m is the angular span of the shell panel.

2.2. Governing equations for a single layer

The constitutive equations take the forms

$$\begin{bmatrix} \sigma_r \\ \sigma_\theta \\ \sigma_z \\ \tau_{\theta z} \\ D_r \end{bmatrix} = \begin{bmatrix} C_{11} & C_{12} & C_{14} & e_{11} \\ C_{12} & C_{22} & C_{24} & e_{12} \\ C_{13} & C_{23} & C_{34} & e_{13} \\ C_{14} & C_{24} & C_{44} & e_{14} \\ e_{11} & e_{12} & e_{14} & -\epsilon_{11} \end{bmatrix} \begin{bmatrix} \varepsilon_r \\ \varepsilon_\theta \\ \gamma_{\theta z} \\ -E_r \end{bmatrix}, \quad \begin{bmatrix} \tau_{rz} \\ \tau_{r\theta} \\ D_\theta \\ D_z \end{bmatrix} = \begin{bmatrix} C_{55} & C_{56} & e_{25} \\ C_{56} & C_{66} & e_{26} \\ e_{25} & e_{26} & -\epsilon_{22} \\ e_{35} & e_{36} & -\epsilon_{23} \end{bmatrix} \begin{bmatrix} \gamma_{rz} \\ \gamma_{r\theta} \\ -E_\theta \end{bmatrix}, \tag{2}$$

where C_{ij}, e_{ij} and ϵ_{ij} are the stiffness coefficients, piezoelectric coefficients and dielectric coefficients of the layer under consideration; D_r, D_θ and D_z are electric displacements; E_r and E_θ are electric fields. If the considered layer is elastic, then $e_{ij} = 0$. The dielectricity equation for an elastic layer, which is decoupled from the elastostatics, is not of interest in this paper. As a result, the dielectric coefficients of the elastic layer are trivial to the deformation of the smart shell. If one orthotropy axis of this layer coincides with the radial axis, while another orthotropy axis of this layer is inclined at an angle α to the longitudinal axis, α being the

positive clockwise, then C_{ij}, e_{ij}, ϵ_{ij} can be expressed in terms of the angle α and $\widetilde{C}_{ij}$, $\tilde{e}_{ij}$, $\tilde{\epsilon}_{ij}$ in a cylindrical coordinate system aligned with the material axes as follows

$$
\begin{aligned}
&C_{11} = \widetilde{C}_{11}, \quad C_{12} = \cos^2\alpha\widetilde{C}_{12} + \sin^2\alpha\widetilde{C}_{13}, \quad C_{13} = \sin^2\alpha\widetilde{C}_{12} + \cos^2\alpha\widetilde{C}_{13}, \quad C_{14} = \sin\alpha\cos\alpha(\widetilde{C}_{12} - \widetilde{C}_{13}),\\
&C_{22} = \cos^4\alpha\widetilde{C}_{22} + 2\sin^2\alpha\cos^2\alpha(\widetilde{C}_{23} + 2\widetilde{C}_{44}) + \sin^4\alpha\widetilde{C}_{33},\\
&C_{23} = \sin^2\alpha\cos^2\alpha(\widetilde{C}_{22} + \widetilde{C}_{33} - 4\widetilde{C}_{44}) + (\sin^4\alpha + \cos^4\alpha)\widetilde{C}_{23},\\
&C_{24} = \sin\alpha\cos^3\alpha(\widetilde{C}_{22} - \widetilde{C}_{23} - 2\widetilde{C}_{44}) + \cos\alpha\sin^3\alpha(\widetilde{C}_{23} - \widetilde{C}_{33} + 2\widetilde{C}_{44}),\\
&C_{34} = \cos\alpha\sin^3\alpha(\widetilde{C}_{22} - \widetilde{C}_{23} - 2\widetilde{C}_{44}) + \sin\alpha\cos^3\alpha(\widetilde{C}_{23} - \widetilde{C}_{33} + 2\widetilde{C}_{44}),\\
&C_{44} = \sin^2\alpha\cos^2\alpha(\widetilde{C}_{22} + \widetilde{C}_{33} - 2\widetilde{C}_{23} - 2\widetilde{C}_{44}) + (\cos^4\alpha + \sin^4\alpha)\widetilde{C}_{44},\\
&C_{55} = \cos^2\alpha\widetilde{C}_{55} + \sin^2\alpha\widetilde{C}_{66}, \quad C_{56} = \sin\alpha\cos\alpha(\widetilde{C}_{66} - \widetilde{C}_{55}), \quad C_{66} = \sin^2\alpha\widetilde{C}_{55} + \cos^2\alpha\widetilde{C}_{66}.
\end{aligned}
\tag{3a}
$$

$$
\begin{aligned}
&e_{11} = \tilde{e}_{11}, \quad e_{12} = \cos^2\alpha\tilde{e}_{12} + \sin^2\alpha\tilde{e}_{13}, \quad e_{13} = \sin^2\alpha\tilde{e}_{12} + \cos^2\alpha\tilde{e}_{13}, \quad e_{14} = \sin\alpha\cos\alpha(\tilde{e}_{12} - \tilde{e}_{13}),\\
&e_{25} = e_{36} = \sin\alpha\cos\alpha(\tilde{e}_{26} - \tilde{e}_{35}), \quad e_{26} = \cos^2\alpha\tilde{e}_{26} + \sin^2\alpha\tilde{e}_{35}, \quad e_{35} = \cos^2\alpha\tilde{e}_{35} + \sin^2\alpha\tilde{e}_{26}.
\end{aligned}
\tag{3b}
$$

$$
\begin{aligned}
&\epsilon_{11} = \tilde{\epsilon}_{11}, \quad \epsilon_{22} = \cos^2\alpha\tilde{\epsilon}_{22} + \sin^2\alpha\tilde{\epsilon}_{33},\\
&\epsilon_{23} = \sin\alpha\cos\alpha(\tilde{\epsilon}_{22} - \tilde{\epsilon}_{33}), \quad \epsilon_{33} = \cos^2\alpha\tilde{\epsilon}_{33} + \sin^2\alpha\tilde{\epsilon}_{22}.
\end{aligned}
\tag{3c}
$$

The relations of strain–displacement and electric field–electric potential ϕ in the cylindrical coordinate system are

$$
\begin{aligned}
&\varepsilon_r = u_{r,r}, \quad \varepsilon_\theta = (u_{\theta,\theta} + u_r)/r, \quad \gamma_{\theta z} = u_{z,\theta}/r,\\
&\gamma_{rz} = u_{z,r}, \quad \gamma_{r\theta} = (u_{r,\theta} - u_\theta)/r + u_{\theta,r},\\
&E_r = -\phi_{,r}, \quad E_\theta = -\phi_{,\theta}/r.
\end{aligned}
\tag{4}
$$

The equations of equilibrium are

$$
\begin{aligned}
&\sigma_{r,r} + \tau_{r\theta,\theta}/r + (\sigma_r - \sigma_\theta)/r = 0,\\
&\tau_{r\theta,r} + \sigma_{\theta,\theta}/r + 2\tau_{r\theta}/r = 0,\\
&\tau_{rz,r} + (\tau_{\theta z,\theta} + \tau_{rz})/r = 0,\\
&D_{r,r} + (D_{\theta,\theta} + D_r)/r = 0.
\end{aligned}
\tag{5}
$$

2.3. The boundary and continuity conditions

The boundary and continuity conditions to be satisfied are those at the longitudinal edges of the smart laminated shell, as well as those on the lateral surfaces and different interfaces of the laminate. These boundary and continuity conditions are specifically listed as follows

(I) Simply-supported edge boundary conditions for each layer

$$
u_r = \sigma_\theta = \tau_{\theta z} = \phi = 0 \quad \text{at } \theta = 0, \theta_m \text{ for each layer.} \tag{6}
$$

(II) Boundary conditions on the outer surface of the piezoelectric actuator

$$
\sigma_r = q_0\sin(p\theta), \quad \tau_{rz} = \tau_{r\theta} = 0, \quad \phi = V_1\sin(p\theta) \quad (r = R_{N+2}). \tag{7}
$$

(III) Boundary conditions on the inner surface of the piezoelectric sensor

$$\sigma_r = \tau_{rz} = \tau_{r\theta} = D_r = 0 \quad (r = R_0). \tag{8}$$

(IV) Linear model for imperfect bonding between two adjacent elastic layers

For imperfectly bonded interface models, the displacements at the interfaces may be discontinuous while the tractions at layer interfaces are always continuous. The continuity of tractions at interfaces can be expressed as

$$\begin{aligned} &\sigma_r(R_j,\theta) = \sigma_r(R_j^-,\theta) = \sigma_r(R_j^+,\theta),\\ &\tau_{rz}(R_j,\theta) = \tau_{rz}(R_j^-,\theta) = \tau_{rz}(R_j^+,\theta), \qquad j = 2,3,\ldots,N,\\ &\tau_{r\theta}(R_j,\theta) = \tau_{r\theta}(R_j^-,\theta) = \tau_{r\theta}(R_j^+,\theta), \end{aligned} \tag{9}$$

where the superscripts "+" and "−" denote the limit values from the exterior and interior sides of the interface $r = R_j$. In this research, linear models (Achenbach and Zhu, 1990; Wang and Meguid, 1999; Liu et al., 2001; Librescu and Schmidt, 2001) are adopted to represent the imperfectly bonded interface conditions. In the linear models, the discontinuities in displacements at the interfaces are assumed to be proportional, in terms of the 'spring-factor-type' interface parameters, to their respective interface traction components. More precisely,

$$\begin{aligned} &\sigma_r(R_j,\theta) = M_j[u_r(R_j^+,\theta) - u_r(R_j^-,\theta)],\\ &\tau_{rz}(R_j,\theta) = \Pi_j[u_z(R_j^+,\theta) - u_z(R_j^-,\theta)], \qquad j = 2,3,\ldots,N,\\ &\tau_{r\theta}(R_j,\theta) = \Theta_j[u_\theta(R_j^+,\theta) - u_\theta(R_j^-,\theta)], \end{aligned} \tag{10}$$

where M_j, Π_j, Θ_j are three non-negative imperfect interface coefficients, and are the bonding stiffness tensor of the interface $r = R_j$ as termed by Librescu and Schmidt (2001).

As M_j, Π_j and $\Theta_j \to \infty$, the interface is perfectly bonded. At the other extreme end, $M_j = \Pi_j = \Theta_j = 0$ represent complete debonding. When only $M_j \to \infty$, while Π_j and Θ_j remain finite, the interface is frictionally bonded. When $M_j \to \infty$, $\Pi_j = \Theta_j = 0$, the interface becomes a frictionless sliding interface or a *perfectly lubricated interface* (Aboudi, 1987; Librescu and Schmidt, 2001).

(V) Boundary and continuity conditions on the sensor/substrate and actuator/substrate interfaces $r = R_1$ and $r = R_{N+1}$

$$\begin{aligned} &\sigma_r(R_j^-,\theta) = \sigma_r(R_j^+,\theta), \quad \tau_{rz}(R_j^-,\theta) = \tau_{rz}(R_j^+,\theta), \quad \tau_{r\theta}(R_j^-,\theta) = \tau_{r\theta}(R_j^+,\theta),\\ &u_r(R_j^-,\theta) = u_r(R_j^+,\theta), \quad u_z(R_j^-,\theta) = u_z(R_j^+,\theta), \quad u_\theta(R_j^-,\theta) = u_\theta(R_j^+,\theta), \qquad j = 1, N+1.\\ &\phi(R_j^+,\theta) = \phi(R_j^-,\theta) = 0. \end{aligned} \tag{11}$$

3. General solution for an elastic layer

Having in view that the dielectric properties and the elastic properties of the elastic layer are irrelevant to each other, the dielectric moduli of the elastic layer have trivial contributions to the elastic deformation of the elastic layer. In this section, only the solution for mechanical quantities, such as displacements and stresses, is presented. In view of (6), the displacement vector can take the following forms

$$\mathbf{U} = \begin{bmatrix} u_r \\ u_\theta \\ u_z \end{bmatrix} = r^s \begin{bmatrix} a_1 \sin(p\theta) \\ a_2 \cos(p\theta) \\ a_3 \cos(p\theta) \end{bmatrix}. \tag{12}$$

Substitution of (12) into (4), and then into the constitutive relations (2) will yield the traction vector as follows

$$\mathbf{t} = \begin{bmatrix} \sigma_r \\ \tau_{r\theta} \\ \tau_{rz} \end{bmatrix} = r^{s-1} \begin{bmatrix} b_1 \sin(p\theta) \\ b_2 \cos(p\theta) \\ b_3 \cos(p\theta) \end{bmatrix}. \tag{13}$$

Introducing two 3×1 vectors $\mathbf{a}$ and $\mathbf{b}$

$$\mathbf{a} = [\, a_1 \quad a_2 \quad a_3 \,]^{\mathrm{T}}, \quad \mathbf{b} = [\, b_1 \quad b_2 \quad b_3 \,]^{\mathrm{T}}, \tag{14}$$

then we can find that the vector $\mathbf{b}$ is related to the vector $\mathbf{a}$ by

$$\mathbf{b} = (-\mathbf{R}^{\mathrm{T}} + s\mathbf{T})\mathbf{a} = -\frac{1}{s}(\mathbf{Q} + s\mathbf{R})\mathbf{a}, \tag{15}$$

where the superscript T denotes matrix transpose, and the three 3×3 real matrices $\mathbf{T}$, $\mathbf{Q}$, $\mathbf{R}$ are defined by

$$\begin{aligned} \mathbf{T} &= \mathbf{T}^{\mathrm{T}} = \begin{bmatrix} C_{11} & 0 & 0 \\ 0 & C_{66} & C_{56} \\ 0 & C_{56} & C_{55} \end{bmatrix}, \\ \mathbf{Q} &= \mathbf{Q}^{\mathrm{T}} = \begin{bmatrix} -(C_{22} + p^2 C_{66}) & p(C_{66} + C_{22}) & pC_{24} \\ p(C_{66} + C_{22}) & -(p^2 C_{22} + C_{66}) & -p^2 C_{24} \\ pC_{24} & -p^2 C_{24} & -p^2 C_{44} \end{bmatrix}, \\ \mathbf{R} &= \begin{bmatrix} -C_{12} & -pC_{66} & -pC_{56} \\ pC_{12} & C_{66} & C_{56} \\ pC_{14} & 0 & 0 \end{bmatrix}. \end{aligned} \tag{16}$$

Meanwhile, the in-plane stresses σ_θ, σ_z, $\tau_{\theta z}$ can be expressed as

$$\begin{bmatrix} \sigma_\theta \\ \sigma_z \\ \tau_{\theta z} \end{bmatrix} = \mathbf{q} r^{s-1} \sin(p\theta), \tag{17}$$

where

$$\mathbf{q} = \begin{bmatrix} C_{12}s + C_{22} & -C_{22}p & -C_{24}p \\ C_{13}s + C_{23} & -C_{23}p & -C_{34}p \\ C_{14}s + C_{24} & -C_{24}p & -C_{44}p \end{bmatrix} \begin{bmatrix} a_1 \\ a_2 \\ a_3 \end{bmatrix}. \tag{18}$$

Now inserting (12) into (4), then into (2), and finally into the equations of equilibrium (5), one can arrive at the following eigenrelations

$$[\mathbf{Q} + s(\mathbf{R} + \mathbf{R}') + s^2\mathbf{T}]\mathbf{a} = \mathbf{0}, \tag{19}$$

where $\mathbf{R}' = -\mathbf{R}^{\mathrm{T}}$. Observing the fact that $\mathbf{R} + \mathbf{R}'$ is an antisymmetric matrix, we can deduce that if s is an eigenvalue of (19), then $-s$ is also an eigenvalue of the eigenequation (19). Eq. (19) can be recast into the following standard eigenrelations

$$\mathbf{N} \begin{bmatrix} \mathbf{a} \\ \mathbf{b} \end{bmatrix} = s \begin{bmatrix} \mathbf{a} \\ \mathbf{b} \end{bmatrix}, \tag{20}$$

where

$$\mathbf{N} = \begin{bmatrix} -\mathbf{T}^{-1}\mathbf{R}' & \mathbf{T}^{-1} \\ -\mathbf{Q} + \mathbf{R}\mathbf{T}^{-1}\mathbf{R}' & -\mathbf{R}\mathbf{T}^{-1} \end{bmatrix}. \tag{21}$$

Assume that the first three eigenvalues of (20) have positive real parts (or positive imaginary parts for purely imaginary roots), the remaining three have opposite signs to the first three. Also we distinguish the six eigenvectors of (20) by attaching a subscript to **a** and **b**. Then the general solution for the displacement vector and the traction vector (of the r-dependent factor) can be concisely expressed as

$$\begin{bmatrix} \mathbf{U} \\ r\mathbf{t} \end{bmatrix} = \begin{bmatrix} \mathbf{A}_1 & \mathbf{A}_2 \\ \mathbf{B}_1 & \mathbf{B}_2 \end{bmatrix} \langle r^{s_\alpha} \rangle \begin{bmatrix} \mathbf{K}_1 \\ \mathbf{K}_2 \end{bmatrix}, \tag{22}$$

where $\mathbf{K}_1$ and $\mathbf{K}_2$ are two 3×1 constant vectors to be determined, and

$$\begin{aligned} &\mathbf{A}_1 = [\,\mathbf{a}_1 \quad \mathbf{a}_2 \quad \mathbf{a}_3\,], \quad \mathbf{A}_2 = [\,\mathbf{a}_4 \quad \mathbf{a}_5 \quad \mathbf{a}_6\,], \\ &\mathbf{B}_1 = [\,\mathbf{b}_1 \quad \mathbf{b}_2 \quad \mathbf{b}_3\,], \quad \mathbf{B}_2 = [\,\mathbf{b}_4 \quad \mathbf{b}_5 \quad \mathbf{b}_6\,], \\ &\langle r^{s_\alpha} \rangle = \mathrm{diag}[\,r^{s_1} \quad r^{s_2} \quad r^{s_3} \quad r^{-s_1} \quad r^{-s_2} \quad r^{-s_3}\,]. \end{aligned} \tag{23}$$

In this section, we have derived the general solution for a single elastic layer in terms of the six-dimensional pseudo-Stroh formalism. Furthermore, the in-plane stresses (of the r-dependent factor) can be expressed in terms of the displacement vector and the traction vector as

$$r \begin{bmatrix} \sigma_\theta \\ \sigma_z \\ \tau_{\theta z} \end{bmatrix} = \begin{bmatrix} E_{11} & -pE_{11} & -pE_{31} & E_{14} & 0 & 0 \\ E_{21} & -pE_{21} & E_{23} & E_{24} & 0 & 0 \\ E_{31} & -pE_{31} & E_{33} & E_{34} & 0 & 0 \end{bmatrix} \begin{bmatrix} \mathbf{U} \\ r\mathbf{t} \end{bmatrix}, \tag{24}$$

where

$$\begin{aligned} &E_{11} = (C_{11}C_{22} - C_{12}^2)/C_{11}, \quad E_{21} = (C_{11}C_{23} - C_{12}C_{13})/C_{11}, \\ &E_{31} = (C_{11}C_{24} - C_{12}C_{14})/C_{11}, \quad E_{23} = p(C_{13}C_{14} - C_{11}C_{34})/C_{11}, \\ &E_{33} = p(C_{14}^2 - C_{11}C_{44})/C_{11}, \quad E_{14} = C_{12}/C_{11}, \\ &E_{24} = C_{13}/C_{11}, \quad E_{34} = C_{14}/C_{11}. \end{aligned} \tag{25}$$

4. General solution for a piezoelectric layer

In view of (6), the extended displacement vector can take the following form

$$\widetilde{\mathbf{U}} = \begin{bmatrix} \mathbf{U} \\ \phi \end{bmatrix} = \begin{bmatrix} u_r \\ u_\theta \\ u_z \\ \phi \end{bmatrix} = r^s \begin{bmatrix} a_1 \sin(p\theta) \\ a_2 \cos(p\theta) \\ a_3 \cos(p\theta) \\ a_4 \sin(p\theta) \end{bmatrix}. \tag{26}$$

Substitution of (26) into (4), and then into the constitutive relations (2) will yield the extended traction vector as follows

$$\tilde{\mathbf{t}} = \begin{bmatrix} \mathbf{t} \\ D_r \end{bmatrix} = \begin{bmatrix} \sigma_r \\ \tau_{r\theta} \\ \tau_{rz} \\ D_r \end{bmatrix} = r^{s-1} \begin{bmatrix} b_1 \sin(p\theta) \\ b_2 \cos(p\theta) \\ b_3 \cos(p\theta) \\ b_4 \sin(p\theta) \end{bmatrix}. \tag{27}$$

Introducing two 4×1 vectors $\tilde{\mathbf{a}}$ and $\tilde{\mathbf{b}}$

$$\tilde{\mathbf{a}} = [\,a_1 \quad a_2 \quad a_3 \quad a_4\,]^{\mathrm{T}}, \quad \tilde{\mathbf{b}} = [\,b_1 \quad b_2 \quad b_3 \quad b_4\,]^{\mathrm{T}}, \tag{28}$$

then we can find that the vector $\tilde{\mathbf{b}}$ is related to the vector $\tilde{\mathbf{a}}$ by

$$\tilde{\mathbf{b}} = (-\widetilde{\mathbf{R}}^{\mathrm{T}} + s\widetilde{\mathbf{T}})\tilde{\mathbf{a}} = -\frac{1}{s}(\widetilde{\mathbf{Q}} + s\widetilde{\mathbf{R}})\tilde{\mathbf{a}}, \tag{29}$$

where the three 4×4 real matrices $\widetilde{\mathbf{T}}$, $\widetilde{\mathbf{Q}}$, $\widetilde{\mathbf{R}}$ are defined by

$$\widetilde{\mathbf{T}}=\widetilde{\mathbf{T}}^{\mathrm{T}}=\begin{bmatrix} C_{11} & 0 & 0 & e_{11}\\ 0 & C_{66} & C_{56} & 0\\ 0 & C_{56} & C_{55} & 0\\ e_{11} & 0 & 0 & -\epsilon_{11}\end{bmatrix},$$

$$\widetilde{\mathbf{Q}}=\widetilde{\mathbf{Q}}^{\mathrm{T}}=\begin{bmatrix} -(C_{22}+p^2C_{66}) & p(C_{66}+C_{22}) & pC_{24} & -p^2e_{26}\\ p(C_{66}+C_{22}) & -(p^2C_{22}+C_{66}) & -p^2C_{24} & pe_{26}\\ pC_{24} & -p^2C_{24} & -p^2C_{44} & 0\\ -p^2e_{26} & pe_{26} & 0 & p^2\epsilon_{22}\end{bmatrix}, \tag{30}$$

$$\widetilde{\mathbf{R}}=\begin{bmatrix} -C_{12} & -pC_{66} & -pC_{56} & -e_{12}\\ pC_{12} & C_{66} & C_{56} & pe_{12}\\ pC_{14} & 0 & 0 & pe_{14}\\ 0 & -pe_{26} & -pe_{25} & 0\end{bmatrix}.$$

In addition, the in-plane stresses σ_θ, σ_z, $\tau_{\theta z}$ and in-plane electric displacements D_θ, D_z can be expressed as

$$\begin{bmatrix}\sigma_\theta\\ \sigma_z\\ \tau_{\theta z}\\ D_\theta\\ D_z\end{bmatrix}=\begin{bmatrix} q_1\sin(p\theta)\\ q_2\sin(p\theta)\\ q_3\sin(p\theta)\\ q_4\cos(p\theta)\\ q_5\cos(p\theta)\end{bmatrix}r^{s-1}, \tag{31}$$

where

$$\begin{bmatrix} q_1\\ q_2\\ q_3\\ q_4\\ q_5\end{bmatrix}=\begin{bmatrix} C_{12}s+C_{22} & -C_{22}p & -C_{24}p & e_{12}s\\ C_{13}s+C_{23} & -C_{23}p & -C_{34}p & e_{13}s\\ C_{14}s+C_{24} & -C_{24}p & -C_{44}p & e_{14}s\\ e_{26}p & e_{26}(s-1) & e_{25}s & -\epsilon_{22}p\\ e_{36}p & e_{36}(s-1) & e_{35}s & -\epsilon_{23}p\end{bmatrix}\begin{bmatrix} a_1\\ a_2\\ a_3\\ a_4\end{bmatrix}. \tag{32}$$

Now inserting (26) into (4), then into (2), and finally into the equations of equilibrium (5), one can arrive at the following eigenrelations

$$\left[\widetilde{\mathbf{Q}}+s(\widetilde{\mathbf{R}}+\widetilde{\mathbf{R}}')+s^2\widetilde{\mathbf{T}}\right]\tilde{\mathbf{a}}=\mathbf{0}, \tag{33}$$

where $\widetilde{\mathbf{R}}'=-\widetilde{\mathbf{R}}^{\mathrm{T}}$. Observing the fact that $\widetilde{\mathbf{R}}+\widetilde{\mathbf{R}}'$ is an antisymmetric matrix, we can deduce that if s is an eigenvalue of (33), then $-s$ is also an eigenvalue of the eigenequation (33). (33) can be recast into the following standard eigenrelations

$$\widetilde{\mathbf{N}}\begin{bmatrix}\tilde{\mathbf{a}}\\ \tilde{\mathbf{b}}\end{bmatrix}=s\begin{bmatrix}\tilde{\mathbf{a}}\\ \tilde{\mathbf{b}}\end{bmatrix}, \tag{34}$$

where

$$\widetilde{\mathbf{N}}=\begin{bmatrix} -\widetilde{\mathbf{T}}^{-1}\widetilde{\mathbf{R}}' & \widetilde{\mathbf{T}}^{-1}\\ -\widetilde{\mathbf{Q}}+\widetilde{\mathbf{R}}\widetilde{\mathbf{T}}^{-1}\widetilde{\mathbf{R}}' & -\widetilde{\mathbf{R}}\widetilde{\mathbf{T}}^{-1}\end{bmatrix}. \tag{35}$$

Assume that the first four eigenvalues of (34) have positive real parts (or positive imaginary parts for purely imaginary roots), the remaining four have opposite signs to the first four. Also we distinguish the eight eigenvectors of (34) by attaching a subscript to $\mathbf{a}$ and $\mathbf{b}$. Then the general solution for the extended

displacement vector and the extended traction vector (of the r-dependent factor) can be concisely expressed as

$$\begin{bmatrix} \widetilde{\mathbf{U}} \\ r\tilde{\mathbf{t}} \end{bmatrix} = \begin{bmatrix} \tilde{\mathbf{A}}_1 & \tilde{\mathbf{A}}_2 \\ \tilde{\mathbf{B}}_1 & \tilde{\mathbf{B}}_2 \end{bmatrix} \langle r^{s_\beta} \rangle \begin{bmatrix} \widetilde{\mathbf{K}}_1 \\ \widetilde{\mathbf{K}}_2 \end{bmatrix}, \tag{36}$$

where $\widetilde{\mathbf{K}}_1$ and $\widetilde{\mathbf{K}}_2$ are two 4×1 constant vectors to be determined, and

$$\begin{aligned} &\tilde{\mathbf{A}}_1 = \begin{bmatrix} \tilde{\mathbf{a}}_1 & \tilde{\mathbf{a}}_2 & \tilde{\mathbf{a}}_3 & \tilde{\mathbf{a}}_4 \end{bmatrix}, \quad \tilde{\mathbf{A}}_2 = \begin{bmatrix} \tilde{\mathbf{a}}_5 & \tilde{\mathbf{a}}_6 & \tilde{\mathbf{a}}_7 & \tilde{\mathbf{a}}_8 \end{bmatrix}, \\ &\tilde{\mathbf{B}}_1 = \begin{bmatrix} \tilde{\mathbf{b}}_1 & \tilde{\mathbf{b}}_2 & \tilde{\mathbf{b}}_3 & \tilde{\mathbf{b}}_4 \end{bmatrix}, \quad \tilde{\mathbf{B}}_2 = \begin{bmatrix} \tilde{\mathbf{b}}_5 & \tilde{\mathbf{b}}_6 & \tilde{\mathbf{b}}_7 & \tilde{\mathbf{b}}_8 \end{bmatrix}, \\ &\langle r^{s_\beta} \rangle = \operatorname{diag}\begin{bmatrix} r^{s_1} & r^{s_2} & r^{s_3} & r^{s_4} & r^{-s_1} & r^{-s_2} & r^{-s_3} & r^{-s_4} \end{bmatrix}. \end{aligned} \tag{37}$$

In this section, we have derived the general solution for a single piezoelectric layer in terms of the eight-dimensional pseudo-Stroh formalism. Meanwhile, the in-plane stresses and in-plane electric displacements (of the r-dependent factor) can be expressed in terms of the extended displacement and the extended traction vectors as

$$r \begin{bmatrix} \sigma_\theta \\ \sigma_z \\ \tau_{\theta z} \\ D_\theta \\ D_z \end{bmatrix} = \begin{bmatrix} \widetilde{E}_{11} & -p\widetilde{E}_{11} & -p\widetilde{E}_{31} & 0 & \widetilde{E}_{15} & 0 & 0 & \widetilde{E}_{18} \\ \widetilde{E}_{21} & -p\widetilde{E}_{21} & \widetilde{E}_{23} & 0 & \widetilde{E}_{25} & 0 & 0 & \widetilde{E}_{28} \\ \widetilde{E}_{31} & -p\widetilde{E}_{31} & \widetilde{E}_{33} & 0 & \widetilde{E}_{35} & 0 & 0 & \widetilde{E}_{38} \\ 0 & 0 & 0 & \widetilde{E}_{44} & 0 & \widetilde{E}_{46} & \widetilde{E}_{47} & 0 \\ 0 & 0 & 0 & \widetilde{E}_{54} & 0 & \widetilde{E}_{56} & \widetilde{E}_{57} & 0 \end{bmatrix} \begin{bmatrix} \widetilde{\mathbf{U}} \\ r\tilde{\mathbf{t}} \end{bmatrix}, \tag{38}$$

where

$$\widetilde{E}_{11} = C_{22} - \frac{C_{12}^2\epsilon_{11} + 2C_{12}e_{11}e_{12} - C_{11}e_{12}^2}{\Delta_1}, \tag{39a}$$

$$\widetilde{E}_{21} = C_{23} - \frac{C_{12}C_{13}\epsilon_{11} + C_{12}e_{11}e_{13} + C_{13}e_{11}e_{12} - C_{11}e_{12}e_{13}}{\Delta_1}, \tag{39b}$$

$$\widetilde{E}_{31} = C_{24} - \frac{C_{12}C_{14}\epsilon_{11} + C_{12}e_{11}e_{14} + C_{14}e_{11}e_{12} - C_{11}e_{12}e_{14}}{\Delta_1}, \tag{39c}$$

$$\widetilde{E}_{23} = -C_{34}p + \frac{p(C_{13}C_{14}\epsilon_{11} + C_{14}e_{11}e_{13} + C_{13}e_{11}e_{14} - C_{11}e_{13}e_{14})}{\Delta_1}, \tag{39d}$$

$$\widetilde{E}_{33} = -pC_{44} + \frac{p(C_{14}^2\epsilon_{11} + 2C_{14}e_{11}e_{14} - C_{11}e_{14}^2)}{\Delta_1}, \tag{39e}$$

$$\widetilde{E}_{44} = -\epsilon_{22}p + \frac{p(2C_{56}e_{25}e_{26} - C_{55}e_{26}e_{26} - C_{66}e_{25}e_{25})}{\Delta_2}, \tag{39f}$$

$$\widetilde{E}_{54} = -\epsilon_{23}p + \frac{p(C_{56}e_{26}e_{35} + C_{56}e_{25}e_{36} - C_{55}e_{26}e_{36} - C_{66}e_{25}e_{35})}{\Delta_2}, \tag{39g}$$

$$\widetilde{E}_{15} = \frac{C_{12}\epsilon_{11} + e_{11}e_{12}}{\Delta_1}, \quad \widetilde{E}_{25} = \frac{C_{13}\epsilon_{11} + e_{11}e_{13}}{\Delta_1}, \quad \widetilde{E}_{35} = \frac{C_{14}\epsilon_{11} + e_{11}e_{14}}{\Delta_1}, \tag{39h}$$

$$\widetilde{E}_{18}=\frac{C_{12}e_{11}-C_{11}e_{12}}{\Delta_1},\quad \widetilde{E}_{28}=\frac{C_{13}e_{11}-C_{11}e_{13}}{\Delta_1},\quad \widetilde{E}_{38}=\frac{C_{14}e_{11}-C_{11}e_{14}}{\Delta_1}, \tag{39i}$$

$$\widetilde{E}_{46}=\frac{C_{55}e_{26}-C_{56}e_{25}}{\Delta_2},\quad \widetilde{E}_{47}=\frac{C_{66}e_{25}-C_{56}e_{26}}{\Delta_2}, \tag{39j}$$

$$\widetilde{E}_{56}=\frac{C_{55}e_{36}-C_{56}e_{35}}{\Delta_2},\quad \widetilde{E}_{57}=\frac{C_{66}e_{35}-C_{56}e_{36}}{\Delta_2}, \tag{39k}$$

where $\Delta_1=C_{11}\epsilon_{11}+e_{11}^2$, $\Delta_2=C_{55}C_{66}-C_{56}^2$.

5. Transfer matrix and solution of layered system

5.1. Transfer matrix for the elastic layers

Due to the fact that the structure of the 6×6 real matrix $\mathbf{N}$ introduced in (21) is identical to that of the 10×10 real matrix $\mathbf{N}$ used in Pan (2001), then the following orthogonal relationship can be similarly derived

$$\begin{bmatrix}-\mathbf{B}_2^{\mathrm{T}} & \mathbf{A}_2^{\mathrm{T}}\\ \mathbf{B}_1^{\mathrm{T}} & -\mathbf{A}_1^{\mathrm{T}}\end{bmatrix}\begin{bmatrix}\mathbf{A}_1 & \mathbf{A}_2\\ \mathbf{B}_1 & \mathbf{B}_2\end{bmatrix}=\begin{bmatrix}\mathbf{I}_{3\times 3} & \mathbf{0}\\ \mathbf{0} & \mathbf{I}_{3\times 3}\end{bmatrix}, \tag{40}$$

where $\mathbf{I}_{3\times 3}$ is a 3×3 unit matrix.

For a certain homogeneous elastic layer $k+1$ with inner radius R_k $(k=1,2,\ldots,N)$, we have the following relation

$$\begin{bmatrix}\mathbf{K}_1\\ \mathbf{K}_2\end{bmatrix}=\langle 1/R_k^{s_\alpha}\rangle\begin{bmatrix}\mathbf{A}_1 & \mathbf{A}_2\\ \mathbf{B}_1 & \mathbf{B}_2\end{bmatrix}^{-1}\begin{bmatrix}\mathbf{U}\\ R_k\mathbf{t}\end{bmatrix}_{R_k^+}=\langle 1/R_k^{s_\alpha}\rangle\begin{bmatrix}-\mathbf{B}_2^{\mathrm{T}} & \mathbf{A}_2^{\mathrm{T}}\\ \mathbf{B}_1^{\mathrm{T}} & -\mathbf{A}_1^{\mathrm{T}}\end{bmatrix}\begin{bmatrix}\mathbf{U}\\ R_k\mathbf{t}\end{bmatrix}_{R_k^+}. \tag{41}$$

Then the solution at any position within this homogeneous layer is related to that at the inner radius R_k as follows

$$\begin{bmatrix}\mathbf{U}\\ r\mathbf{t}\end{bmatrix}=\mathbf{P}_k(r/R_k)\begin{bmatrix}\mathbf{U}\\ R_k\mathbf{t}\end{bmatrix}_{R_k^+}\quad (k=1,2,\ldots,N), \tag{42}$$

where

$$\mathbf{P}_k(r/R_k)=\begin{bmatrix}\mathbf{A}_1 & \mathbf{A}_2\\ \mathbf{B}_1 & \mathbf{B}_2\end{bmatrix}\langle (r/R_k)^{s_\alpha}\rangle\begin{bmatrix}-\mathbf{B}_2^{\mathrm{T}} & \mathbf{A}_2^{\mathrm{T}}\\ \mathbf{B}_1^{\mathrm{T}} & -\mathbf{A}_1^{\mathrm{T}}\end{bmatrix} \tag{43}$$

is the field transfer matrix for the elastic layer. It is proved in the Appendix A that the field transfer matrix can be directly determined from the real matrix $\mathbf{N}$ defined by (21), thus the calculation of the eigenvectors of (20) can be circumvented. Furthermore, the linearly imperfect bonding interface model (10) can be equivalently expressed as

$$\begin{bmatrix}\mathbf{U}\\ R_k\mathbf{t}\end{bmatrix}_{R_k^+}=\mathbf{F}_k\begin{bmatrix}\mathbf{U}\\ R_k\mathbf{t}\end{bmatrix}_{R_k^-}\quad (k=2,3,\ldots,N), \tag{44}$$

where

$$\mathbf{F}_k = \begin{bmatrix} 1 & 0 & 0 & 1/(R_k M_k) & 0 & 0 \\ 0 & 1 & 0 & 0 & 1/(R_k \Theta_k) & 0 \\ 0 & 0 & 1 & 0 & 0 & 1/(R_k \Pi_k) \\ 0 & 0 & 0 & 1 & 0 & 0 \\ 0 & 0 & 0 & 0 & 1 & 0 \\ 0 & 0 & 0 & 0 & 0 & 1 \end{bmatrix} \tag{45}$$

is the point transfer matrix. Consequently, the solution at the interface $r = R_{N+1}^-$ of the shell can be expressed by that at the interface $r = R_1^+$ of the shell as follows

$$\begin{bmatrix} \mathbf{U} \\ R_{N+1}\mathbf{t} \end{bmatrix}_{R_{N+1}^-} = \Omega \begin{bmatrix} \mathbf{U} \\ R_1\mathbf{t} \end{bmatrix}_{R_1^+}, \tag{46}$$

where

$$\begin{aligned} &\Omega = \mathbf{P}_N(\lambda_N) \times \mathbf{F}_N \times \mathbf{P}_{N-1}(\lambda_{N-1}) \times \mathbf{F}_{N-1} \times \cdots \times \mathbf{P}_2(\lambda_2) \times \mathbf{F}_2 \times \mathbf{P}_1(\lambda_1), \\ &\lambda_k = R_{k+1}/R_k \quad (1 \leqslant k \leqslant N). \end{aligned} \tag{47}$$

5.2. Transfer matrix for the piezoelectric layers

Due to the fact that the structure of the 8×8 real matrix $\widetilde{\mathbf{N}}$ introduced in (35) is identical to that of the 10×10 real matrix $\mathbf{N}$ used in Pan (2001), then the following orthogonal relationship can be similarly derived

$$\begin{bmatrix} -\widetilde{\mathbf{B}}_2^{\mathrm{T}} & \tilde{\mathbf{A}}_2^{\mathrm{T}} \\ \widetilde{\mathbf{B}}_1^{\mathrm{T}} & -\tilde{\mathbf{A}}_1^{\mathrm{T}} \end{bmatrix} \begin{bmatrix} \tilde{\mathbf{A}}_1 & \tilde{\mathbf{A}}_2 \\ \widetilde{\mathbf{B}}_1 & \widetilde{\mathbf{B}}_2 \end{bmatrix} = \begin{bmatrix} \mathbf{I}_{4\times4} & \mathbf{0} \\ \mathbf{0} & \mathbf{I}_{4\times4} \end{bmatrix}, \tag{48}$$

where $\mathbf{I}_{4\times4}$ is a 4×4 unit matrix.

For any piezoelectric layer $k+1$ with inner radius R_k $(k = 0, N+1)$, we have the following relation

$$\begin{bmatrix} \widetilde{\mathbf{K}}_1 \\ \widetilde{\mathbf{K}}_2 \end{bmatrix} = \langle 1/R_k^{s_\beta} \rangle \begin{bmatrix} \tilde{\mathbf{A}}_1 & \tilde{\mathbf{A}}_2 \\ \widetilde{\mathbf{B}}_1 & \widetilde{\mathbf{B}}_2 \end{bmatrix}^{-1} \begin{bmatrix} \widetilde{\mathbf{U}} \\ R_k\tilde{\mathbf{t}} \end{bmatrix}_{R_k^+} = \langle 1/R_k^{s_\beta} \rangle \begin{bmatrix} -\widetilde{\mathbf{B}}_2^{\mathrm{T}} & \tilde{\mathbf{A}}_2^{\mathrm{T}} \\ \widetilde{\mathbf{B}}_1^{\mathrm{T}} & -\tilde{\mathbf{A}}_1^{\mathrm{T}} \end{bmatrix} \begin{bmatrix} \widetilde{\mathbf{U}} \\ R_k\tilde{\mathbf{t}} \end{bmatrix}_{R_k^+}. \tag{49}$$

Then the solution at any position within this homogeneous layer is related to that at the inner radius R_k as follows

$$\begin{bmatrix} \widetilde{\mathbf{U}} \\ r\tilde{\mathbf{t}} \end{bmatrix} = \widetilde{\mathbf{P}}_k(r/R_k) \begin{bmatrix} \widetilde{\mathbf{U}} \\ R_k\tilde{\mathbf{t}} \end{bmatrix}_{R_k^+} \quad (k = 0, N+1), \tag{50}$$

where

$$\widetilde{\mathbf{P}}_k(r/R_k) = \begin{bmatrix} \tilde{\mathbf{A}}_1 & \tilde{\mathbf{A}}_2 \\ \widetilde{\mathbf{B}}_1 & \widetilde{\mathbf{B}}_2 \end{bmatrix} \langle (r/R_k)^{s_\beta} \rangle \begin{bmatrix} -\widetilde{\mathbf{B}}_2^{\mathrm{T}} & \tilde{\mathbf{A}}_2^{\mathrm{T}} \\ \widetilde{\mathbf{B}}_1^{\mathrm{T}} & -\tilde{\mathbf{A}}_1^{\mathrm{T}} \end{bmatrix} \tag{51}$$

is the transfer matrix for the piezoelectric layer. It can also be similarly proved that the transfer matrix for the piezoelectric layer can be directly determined from the real matrix $\widetilde{\mathbf{N}}$ defined by (35), thus the calculation of the eigenvectors of (34) can be circumvented. Consequently, the solution at the outer surface of the piezoelectric layer $r = R_{k+1}^-$ can be expressed by that at the inner surface $r = R_k^+$ of the piezoelectric layer as follows

$$\begin{bmatrix} \widetilde{\mathbf{U}} \\ R_{k+1}\tilde{\mathbf{t}} \end{bmatrix}_{R_{k+1}^-} = \widetilde{\mathbf{P}}_k(\lambda_k) \begin{bmatrix} \widetilde{\mathbf{U}} \\ R_k\tilde{\mathbf{t}} \end{bmatrix}_{R_k^+} \quad (k = 0, N+1), \tag{52}$$

where $\lambda_k = R_{k+1}/R_k$ $(k = 0, N+1)$. The above result (52) cannot be used directly due to the appearance of the dielectric quantities ϕ and D_r. To address this problem, $\widetilde{\mathbf{P}}_0(\lambda_0)$ and $\widetilde{\mathbf{P}}_{N+1}(\lambda_{N+1})$ are rewritten into the following partitioned forms

$$\widetilde{\mathbf{P}}_{N+1}(\lambda_{N+1}) = \begin{bmatrix} \mathbf{Y}_{11} & \mathbf{Y}_{12} & \mathbf{Y}_{13} & \mathbf{Y}_{14} \\ \mathbf{Y}_{21} & Y_{22} & \mathbf{Y}_{23} & Y_{24} \\ \mathbf{Y}_{31} & \mathbf{Y}_{32} & \mathbf{Y}_{33} & \mathbf{Y}_{34} \\ \mathbf{Y}_{41} & Y_{42} & \mathbf{Y}_{43} & Y_{44} \end{bmatrix}, \quad \widetilde{\mathbf{P}}_0(\lambda_0) = \begin{bmatrix} \widetilde{\mathbf{Y}}_{11} & \widetilde{\mathbf{Y}}_{12} & \widetilde{\mathbf{Y}}_{13} & \widetilde{\mathbf{Y}}_{14} \\ \widetilde{\mathbf{Y}}_{21} & \widetilde{Y}_{22} & \widetilde{\mathbf{Y}}_{23} & \widetilde{Y}_{24} \\ \widetilde{\mathbf{Y}}_{31} & \widetilde{\mathbf{Y}}_{32} & \widetilde{\mathbf{Y}}_{33} & \widetilde{\mathbf{Y}}_{34} \\ \widetilde{\mathbf{Y}}_{41} & \widetilde{Y}_{42} & \widetilde{\mathbf{Y}}_{43} & \widetilde{Y}_{44} \end{bmatrix}, \tag{53}$$

where $\mathbf{Y}_{11}$, $\mathbf{Y}_{13}$, $\mathbf{Y}_{31}$, $\mathbf{Y}_{33}$ are 3×3 matrices; $\mathbf{Y}_{12}$, $\mathbf{Y}_{14}$, $\mathbf{Y}_{32}$, $\mathbf{Y}_{34}$ are 3×1 matrices; $\mathbf{Y}_{21}$, $\mathbf{Y}_{23}$, $\mathbf{Y}_{41}$, $\mathbf{Y}_{43}$ are 1×3 matrices; Y_{22}, Y_{24}, Y_{42}, Y_{44} are scalars. Identical partitions hold for $\widetilde{\mathbf{P}}_0(\lambda_0)$.

In view of the fact that $\phi = 0$ on $r = R_1$, R_{N+1} and the fact that $D_r = 0$ on $r = R_0$, $\phi = V_1 \sin(p\theta)$ on $r = R_{N+2}$, then it follows from (52) that

$$\begin{aligned} R_{N+1}D_r(R_{N+1}^+) &= -Y_{24}^{-1}\mathbf{Y}_{21}\mathbf{U}(R_{N+1}^+) - Y_{24}^{-1}\mathbf{Y}_{23}R_{N+1}\mathbf{t}(R_{N+1}^+) + Y_{24}^{-1}V_1, \\ \phi(R_0^+) &= -\widetilde{Y}_{22}^{-1}\widetilde{\mathbf{Y}}_{21}\mathbf{U}(R_0^+) - \widetilde{Y}_{22}^{-1}\widetilde{\mathbf{Y}}_{23}R_0\mathbf{t}(R_0^+). \end{aligned} \tag{54}$$

Making use of the above result, (52) can then be rewritten into

$$\begin{bmatrix} \mathbf{U} \\ R_{N+2}\mathbf{t} \end{bmatrix}_{R_{N+2}^-} = \mathbf{P}_{N+1}(\lambda_{N+1}) \begin{bmatrix} \mathbf{U} \\ R_{N+1}\mathbf{t} \end{bmatrix}_{R_{N+1}^+} + V_1 \begin{bmatrix} Y_{24}^{-1}\mathbf{Y}_{14} \\ Y_{24}^{-1}\mathbf{Y}_{34} \end{bmatrix}, \tag{55}$$

$$\begin{bmatrix} \mathbf{U} \\ R_1\mathbf{t} \end{bmatrix}_{R_1^-} = \mathbf{P}_0(\lambda_0) \begin{bmatrix} \mathbf{U} \\ R_0\mathbf{t} \end{bmatrix}_{R_0^+}, \tag{56}$$

where

$$\begin{aligned} \mathbf{P}_{N+1}(\lambda_{N+1}) &= \begin{bmatrix} \mathbf{Y}_{11} - Y_{24}^{-1}\mathbf{Y}_{14}\mathbf{Y}_{21} & \mathbf{Y}_{13} - Y_{24}^{-1}\mathbf{Y}_{14}\mathbf{Y}_{23} \\ \mathbf{Y}_{31} - Y_{24}^{-1}\mathbf{Y}_{34}\mathbf{Y}_{21} & \mathbf{Y}_{33} - Y_{24}^{-1}\mathbf{Y}_{34}\mathbf{Y}_{23} \end{bmatrix}, \\ \mathbf{P}_0(\lambda_0) &= \begin{bmatrix} \widetilde{\mathbf{Y}}_{11} - \widetilde{Y}_{22}^{-1}\widetilde{\mathbf{Y}}_{12}\widetilde{\mathbf{Y}}_{21} & \widetilde{\mathbf{Y}}_{13} - \widetilde{Y}_{22}^{-1}\widetilde{\mathbf{Y}}_{12}\widetilde{\mathbf{Y}}_{23} \\ \widetilde{\mathbf{Y}}_{31} - \widetilde{Y}_{22}^{-1}\widetilde{\mathbf{Y}}_{32}\widetilde{\mathbf{Y}}_{21} & \widetilde{\mathbf{Y}}_{33} - \widetilde{Y}_{22}^{-1}\widetilde{\mathbf{Y}}_{32}\widetilde{\mathbf{Y}}_{23} \end{bmatrix}. \end{aligned} \tag{57}$$

Consequently, the unknown dielectric quantities do not appear in Eqs. (55) and (56).

5.3. Solution of the smart laminated system

Applying Eqs. (11), (46), (55) and (56), we arrive at

$$\begin{bmatrix} \mathbf{U} \\ R_{N+2}\mathbf{t} \end{bmatrix}_{R_{N+2}^-} = \mathbf{P}_{N+1}(\lambda_{N+1}) \times \Omega \times \mathbf{P}_0(\lambda_0) \begin{bmatrix} \mathbf{U} \\ R_0\mathbf{t} \end{bmatrix}_{R_0^+} + V_1 \begin{bmatrix} Y_{24}^{-1}\mathbf{Y}_{14} \\ Y_{24}^{-1}\mathbf{Y}_{34} \end{bmatrix}. \tag{58}$$

Displacement vectors on the two surfaces $r = R_0$, R_{N+2} are the unknowns in the above expression. In view of (8), then (58) can be further reduced to

$$\begin{bmatrix} \mathbf{U}(R_{N+2}^-) \\ R_{N+2}\mathbf{t}(R_{N+2}^-) \end{bmatrix} = \begin{bmatrix} \mathbf{Z}_1 & \mathbf{Z}_2 \\ \mathbf{Z}_3 & \mathbf{Z}_4 \end{bmatrix} \begin{bmatrix} \mathbf{U}(R_0^+) \\ \mathbf{0} \end{bmatrix} + V_1 \begin{bmatrix} Y_{24}^{-1}\mathbf{Y}_{14} \\ Y_{24}^{-1}\mathbf{Y}_{34} \end{bmatrix}, \tag{59}$$

where

$$\begin{bmatrix} \mathbf{Z}_1 & \mathbf{Z}_2 \\ \mathbf{Z}_3 & \mathbf{Z}_4 \end{bmatrix} = \mathbf{P}_{N+1}(\lambda_{N+1}) \times \Omega \times \mathbf{P}_0(\lambda_0). \tag{60}$$

By solving (59), the unknown displacement vectors on the two surfaces can be obtained as

$$\begin{aligned} \mathbf{U}(R_0^+) &= R_{N+2}\mathbf{Z}_3^{-1}\mathbf{t}(R_{N+2}^-) - VY_{24}^{-1}\mathbf{Z}_3^{-1}\mathbf{Y}_{34}, \\ \mathbf{U}(R_{N+2}^-) &= R_{N+2}\mathbf{Z}_1\mathbf{Z}_3^{-1}\mathbf{t}(R_{N+2}^-) + VY_{24}^{-1}(\mathbf{Y}_{14} - \mathbf{Z}_1\mathbf{Z}_3^{-1}\mathbf{Y}_{34}). \end{aligned} \tag{61}$$

The displacement vector and traction vector at any position within the $(k+1)$th $(1 \leqslant k \leqslant N)$ elastic layer of the laminated shell can then be expressed as

$$\begin{bmatrix} \mathbf{U} \\ r\mathbf{t} \end{bmatrix}_r = \mathbf{P}_k(r/R_k) \times \mathbf{F}_k \times \mathbf{P}_{k-1}(\lambda_{k-1}) \times \mathbf{F}_{k-1} \times \cdots\cdots \times \mathbf{P}_2(\lambda_2) \times \mathbf{F}_2 \times \mathbf{P}_1(\lambda_1) \times \mathbf{P}_0(\lambda_0) \begin{bmatrix} \mathbf{U} \\ R_0\mathbf{t} \end{bmatrix}_{R_0^+}, \quad R_k < r < R_{k+1} \quad (1 \leqslant k \leqslant N). \tag{62}$$

The extended displacement vector and the extended traction vector at any position within the bottom piezoelectric sensor of the laminated shell can then be expressed as

$$\begin{bmatrix} \widetilde{\mathbf{U}} \\ r\tilde{\mathbf{t}} \end{bmatrix} = \widetilde{\mathbf{P}}_0(r/R_0) \begin{bmatrix} \mathbf{I}_{3\times3} & \mathbf{0}_{3\times3} \\ -\widetilde{Y}_{22}^{-1}\widetilde{\mathbf{Y}}_{21} & -\widetilde{Y}_{22}^{-1}\widetilde{\mathbf{Y}}_{23} \\ \mathbf{0}_{3\times3} & \mathbf{I}_{3\times3} \\ \mathbf{0}_{1\times3} & \mathbf{0}_{1\times3} \end{bmatrix} \begin{bmatrix} \mathbf{U} \\ r\mathbf{t} \end{bmatrix}_{R_0^+}, \quad R_0 < r < R_1. \tag{63}$$

The extended displacement vector and extended traction vector at any position within the top piezoelectric actuator of the laminated shell can then be expressed as

$$\begin{bmatrix} \widetilde{\mathbf{U}} \\ r\tilde{\mathbf{t}} \end{bmatrix} = \widetilde{\mathbf{P}}_{N+1}(r/R_{N+1}) \left\{ \begin{bmatrix} \mathbf{I}_{3\times3} & \mathbf{0}_{3\times3} \\ \mathbf{0}_{1\times3} & \mathbf{0}_{1\times3} \\ \mathbf{0}_{3\times3} & \mathbf{I}_{3\times3} \\ -Y_{24}^{-1}\mathbf{Y}_{21} & -Y_{24}^{-1}\mathbf{Y}_{23} \end{bmatrix} \times \Omega \times \mathbf{P}_0(\lambda_0) \begin{bmatrix} \mathbf{U} \\ R_0\mathbf{t} \end{bmatrix}_{R_0^+} + \begin{bmatrix} \mathbf{0}_{7\times1} \\ Y_{24}^{-1}V_1 \end{bmatrix} \right\}, \quad R_{N+1} < r < R_{N+2}. \tag{64}$$

Now that the above expressions for displacement vector and traction vector satisfy the governing equations, interfacial conditions and boundary conditions. With the displacement and traction vectors at a given position within the elastic layers being determined, the in-plane stresses in these elastic layers can be evaluated by using (24). With the extended displacement and traction vectors at a given position within the two piezoelectric layers being determined, the in-plane stresses and in-plane electric displacements in the two piezoelectric layers can be evaluated by using (38).

6. Numerical results

In the numerical example, the material of the top actuator and the bottom sensor is taken as the PZT-5A. The symmetry axis of the piezoelectric PZT-5A is along the r-axis with the material properties being listed as follows (Reddy and Cheng, 2001)

$$C_{11} = 86.856 \times 10^9 \text{ N/m}^2,\ C_{22} = C_{33} = 99.201 \times 10^9 \text{ N/m}^2,\ C_{23} = 54.016 \times 10^9 \text{ N/m}^2,$$
$$C_{13} = C_{12} = 50.778 \times 10^9 \text{ N/m}^2,\ C_{44} = 22.60 \times 10^9 \text{ N/m}^2,\ C_{55} = C_{66} = 21.1 \times 10^9 \text{ N/m}^2,$$
$$e_{11} = 15.118 \text{ C/m}^2,\ e_{12} = e_{13} = -7.209 \text{ C/m}^2,\ e_{26} = e_{35} = 12.322 \text{ C/m}^2,$$
$$\epsilon_{11} = 1.5 \times 10^{-8} \text{ N/m}^2,\ \epsilon_{22} = \epsilon_{33} = 1.53 \times 10^{-8} \text{ N/m}^2.$$

Since the top actuator and the bottom sensor are cylindrically isotropic, the material constants will remain unchanged in the new coordinate system when undergoing a coordinate rotation about the radial direction.

The material properties of the graphite/epoxy composite are (Ren, 1987)

$$E_L = 172 \times 10^9 \text{ N/m}^2,\ E_T = 6.9 \times 10^9 \text{ N/m}^2,$$
$$G_{LT} = 3.4 \times 10^9 \text{ N/m}^2,\ G_{TT} = 1.4 \times 10^9 \text{N/m}^2,\ v_{LT} = v_{TT} = 0.25,$$

where L is the direction parallel to the fibers and T is the transverse direction. A three-layered (60°/−60°/60°) graphite/epoxy substrate integrated with PZT-5A actuator and sensor is considered. The imperfect interface parameters are taken to be (Dvorak and Zhang, 2001)

$$M_2 = M_3 = 10^8 \text{ N/m}^3,\ \Pi_2 = \Pi_3 = \Theta_2 = \Theta_3 = 10^9 \text{ N/m}^3.$$

The geometric and loading parameters are assumed to be

$$\theta_m = 1 \text{ rad},\ m = 1.$$

The inner radius of the shell is taken to be unit, i.e., $R_0 = 1$ m, and the thickness of each piezoelectric or elastic layer is 0.2 m. Figs. 2–7 illustrate the variations (the solid lines) of $u_r^* = u_r/\sin(p\theta)$, $u_\theta^* = u_\theta/\cos(p\theta)$, $u_z^* = u_z/\cos(p\theta)$, $\sigma_r^* = \sigma_r/\sin(p\theta)$, $\tau_{r\theta}^* = \tau_{r\theta}/\cos(p\theta)$, $\tau_{rz}^* = \tau_{rz}/\cos(p\theta)$, all of which are independent of the angle θ, along the radial direction when the smart cylindrical shell is only subjected to the electric loads $V_1 = 1$ V and $q_0 = 0$. The corresponding results (the dashed lines) for perfect interfaces are also presented as a comparison. It is observed that all the three displacement components undergo jumps when crossing the

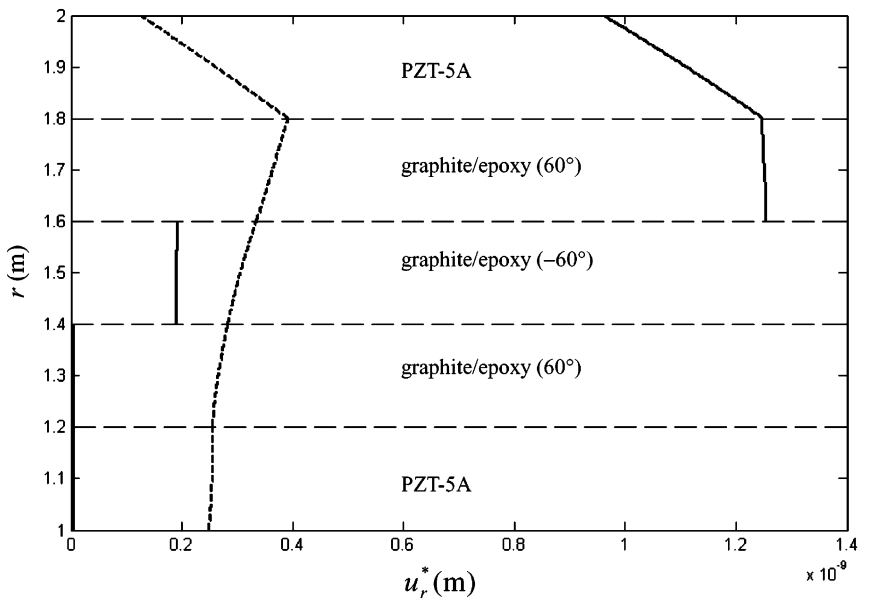

Fig. 2. Variation of u_r^* along the radial direction under electric loads (solid and dashed lines are for the imperfect and perfect interfaces, respectively).

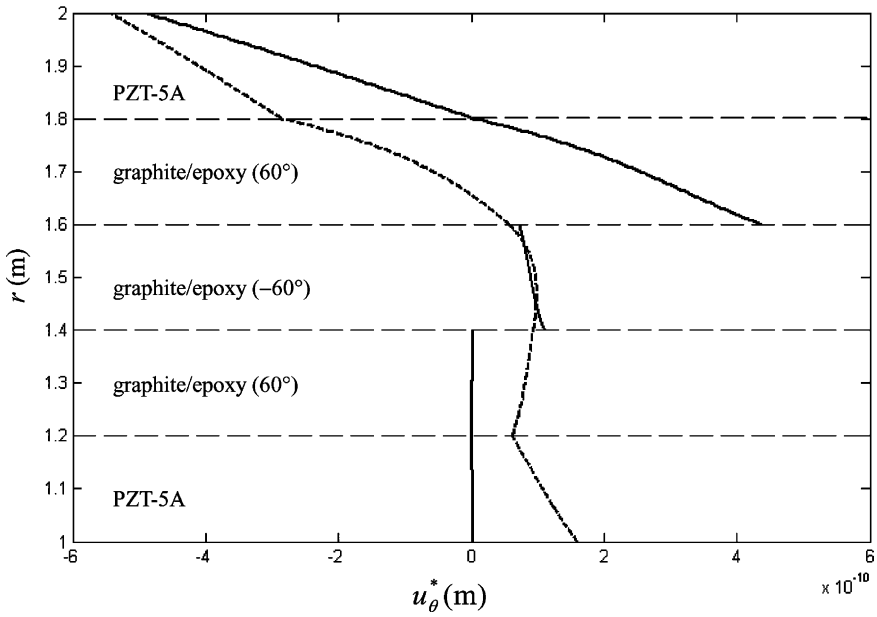

Fig. 3. Variation of u_θ^* along the radial direction under electric loads (solid and dashed lines are for the imperfect and perfect interfaces, respectively).

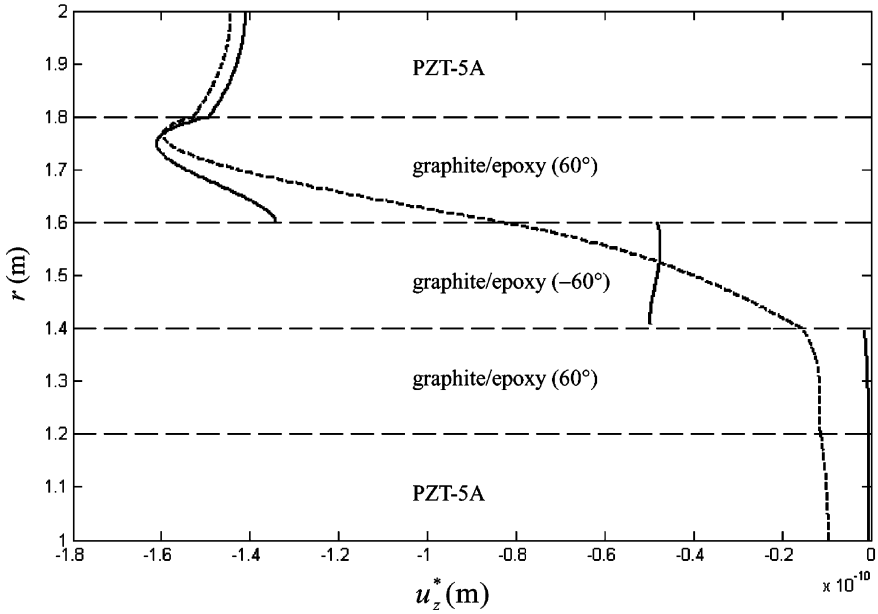

Fig. 4. Variation of u_z^* along the radial direction under electric loads (solid and dashed lines are for the imperfect and perfect interfaces, respectively).

imperfect interfaces separating two elastic layers. Moreover, it has been checked that the jumps in displacements and the corresponding traction components just satisfy the linear models described by Eq. (10). It is observed from Fig. 2 that the physically unacceptable interpenetration phenomenon between

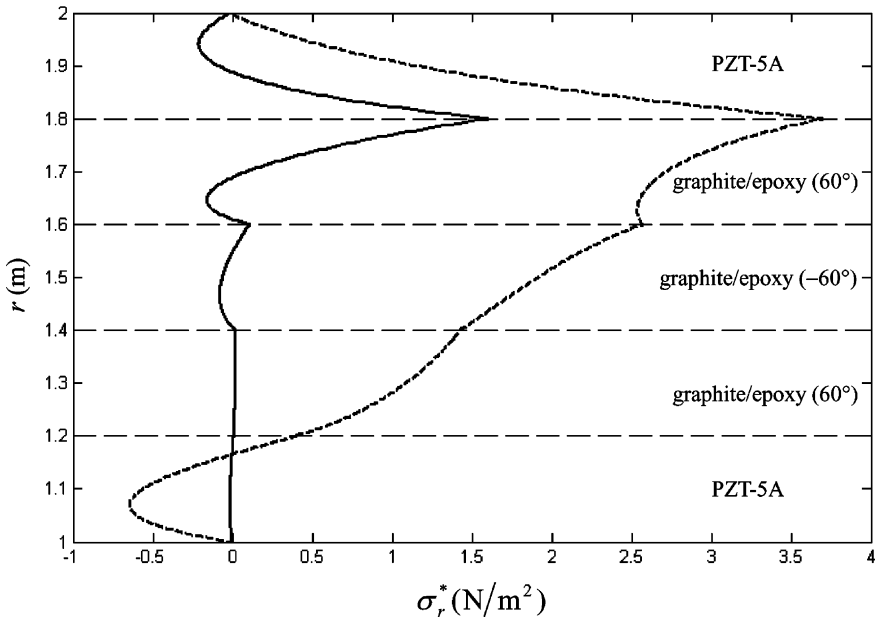

Fig. 5. Variation of σ_r^* along the radial direction under electric loads (solid and dashed lines are for the imperfect and perfect interfaces, respectively).

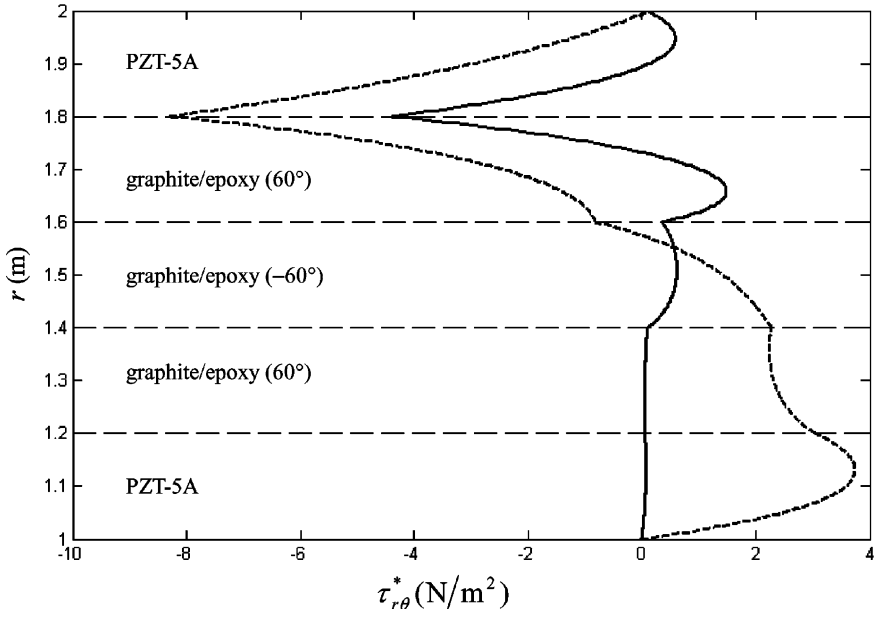

Fig. 6. Variation of $\tau_{r\theta}^*$ along the radial direction under electric loads (solid and dashed lines are for the imperfect and perfect interfaces, respectively).

neighboring constituents (Achenbach and Zhu, 1990) does not occur when the composite is subjected to this kind of electric loads. Figs. 5–7 demonstrate that the presence of the imperfect interfaces can relax the

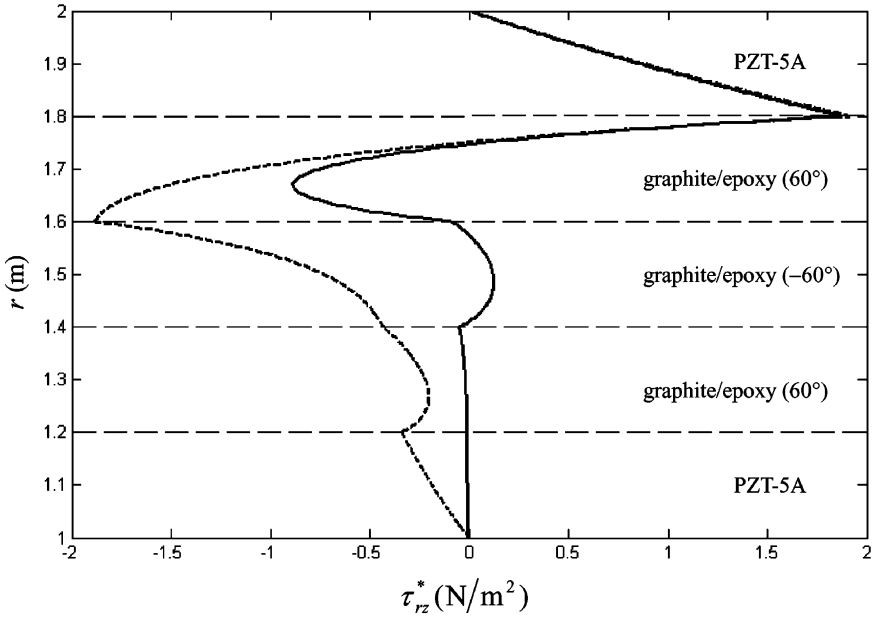

Fig. 7. Variation of τ_{rz}^{*} along the radial direction under electric loads (solid and dashed lines are for the imperfect and perfect interfaces, respectively).

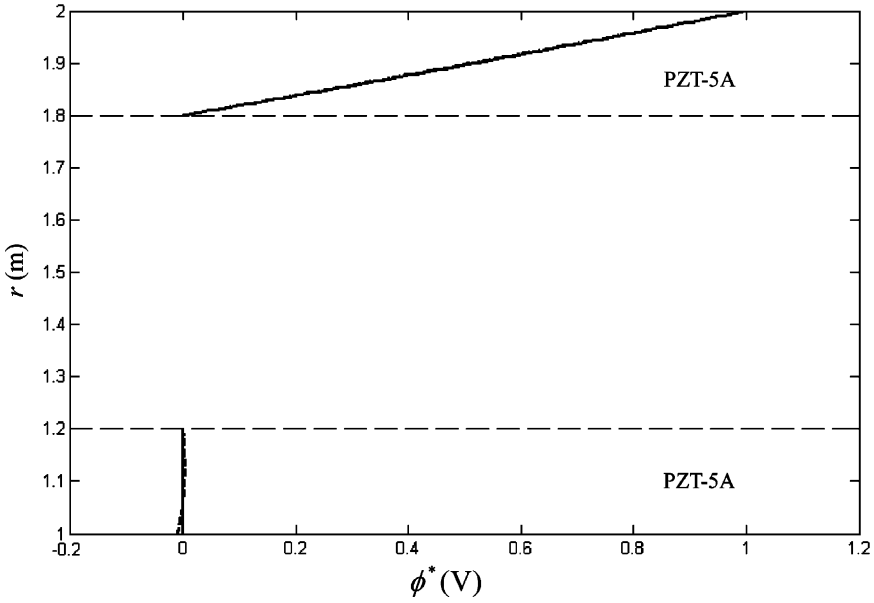

Fig. 8. Variation of ϕ^{*} in the sensor and actuator along the radial direction under electric loads (solid and dashed lines are for the imperfect and perfect interfaces, respectively).

interlaminar stress level. The existence of imperfect interfaces is equivalent to relaxation of interfacial bonding strength, and hence reduction in the overall rigidity of the shells. Figs. 2–7 confirms that the

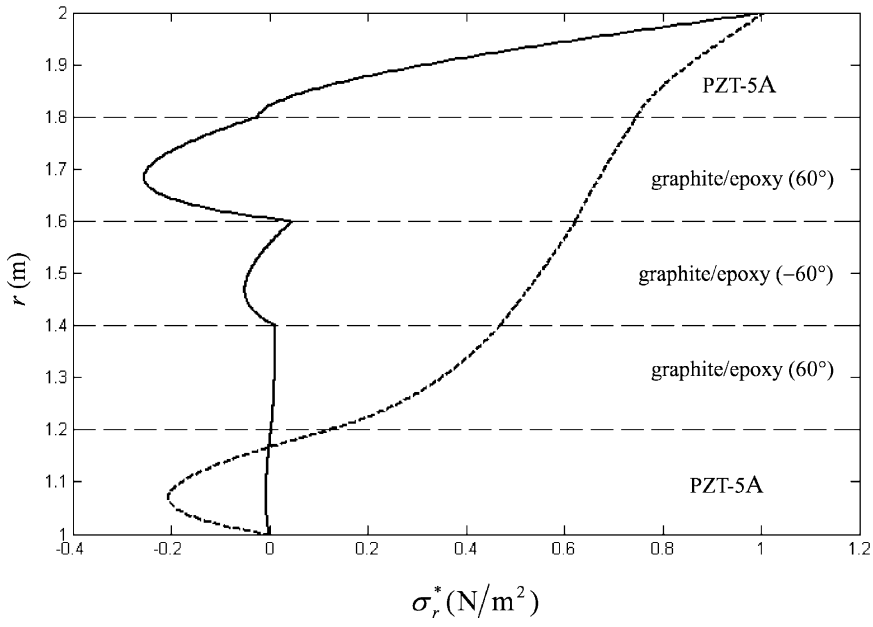

Fig. 9. Variation of σ_r^* along the radial direction under mechanical loads (solid and dashed lines are for the imperfect and perfect interfaces, respectively).

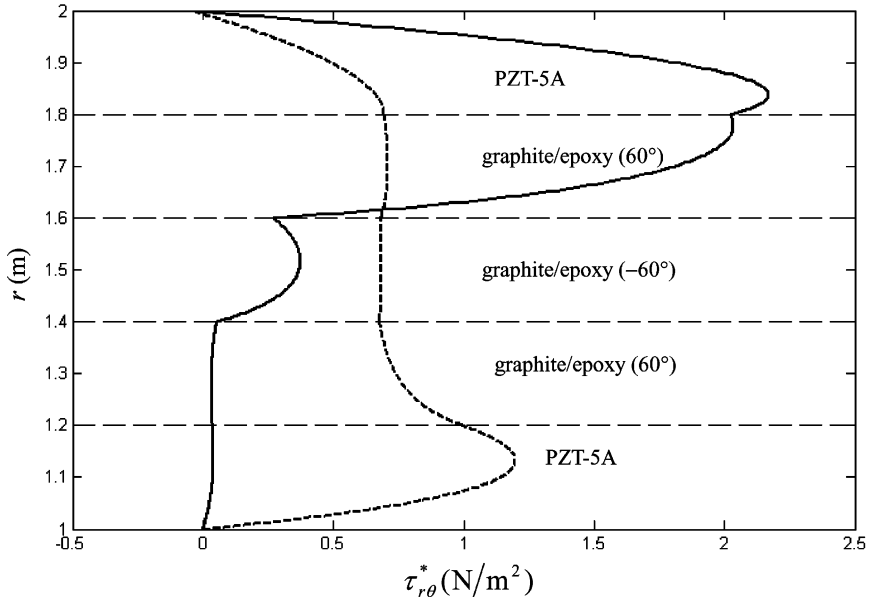

Fig. 10. Variation of $\tau_{r\theta}^*$ along the radial direction under mechanical loads (solid and dashed lines are for the imperfect and perfect interfaces, respectively).

existence of imperfect interfaces will cause reductions in interface stresses but at the expense of increases of the central deflection. Fig. 8 demonstrates the variations of $\phi^* = \phi/\sin(p\theta)$ in the bottom sensor and top

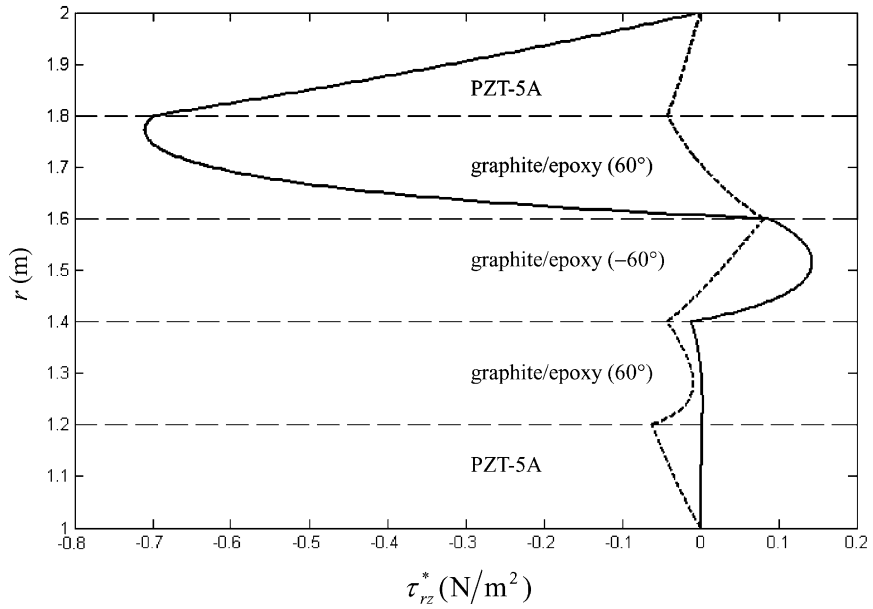

Fig. 11. Variation of τ_{rz}^{*} along the radial direction under mechanical loads (solid and dashed lines are for the imperfect and perfect interfaces, respectively).

actuator along the radial direction under the electric loads $V_1 = 1$ V and $q_0 = 0$. The magnitude of electric potential in the sensor is very small; while the electric potential is nearly a linear function along the radial direction. The interface imperfection has a minimal influence on electric potential. Figs. 9–11 present the variations of σ_r^{*}, $\tau_{r\theta}^{*}$, τ_{rz}^{*} along the radial direction when the smart laminated shell is under mechanical loads $q_0 = 1$ N/m^2 and $V_1 = 0$. It is observed from Figs. 9–11 that even though the existence of the imperfect interfaces can significantly reduce the level of normal stress σ_r^{*} within each layer of the smart laminated shell, the magnitudes of shear stresses $\tau_{r\theta}^{*}$ and τ_{rz}^{*} in the top actuator and in the adjacent elastic layer for the case of imperfect interfaces are much higher than those for the case of perfect interfaces. Consequently, delamination between the actuator and the layered substrate may occur when the interfaces between two adjacent elastic layers are imperfect and when the smart laminated shell is subjected to mechanical loads.

7. Conclusion

Based on the pseudo-Stroh formalism and the transfer matrix method, this paper presents a three-dimensional electroelastic solution for angle-ply cylindrical shells with imperfect bonding at the elastic layer interfaces and with mounted anisotropic piezoelectric layers. The spring-like interface model is utilized here to simulate the imperfectly bonded interfaces between two adjacent elastic layers. Compact and explicit form expressions for all of the field quantities including the in-plane stresses and in-plane electric displacements are given. During the formulation, we take $r\sigma_r$, $r\tau_{r\theta}$, $r\tau_{rz}$ instead of σ_r, $\tau_{r\theta}$, τ_{rz} as the stress variables and rD_r instead of D_r as the electric displacement variable to make the formulation simple and elegant. This novel usage has also been employed by Tarn (2002a,b) in the analysis of cylindrically anisotropic elastic and piezoelectric body.

Acknowledgements

The authors are greatly indebted to two referees for their very helpful comments and suggestions on revising the manuscript. This research was supported by China Postdoctoral Science Foundation.

Appendix A

Defining

$$\Lambda = \mathrm{diag}[\, s_1 \quad s_2 \quad s_3 \quad -s_1 \quad -s_2 \quad -s_3 \,], \tag{A.1}$$

then the 6×6 diagonal matrix $\langle (r/R_k)^{s_\alpha} \rangle$ can be uniquely expressed in terms of Λ^0, Λ^1, Λ^2, Λ^3, Λ^4, Λ^5 as follows

$$\langle (r/R_k)^{s_\alpha} \rangle = \chi_0 \mathbf{I} + \chi_1 \Lambda + \chi_2 \Lambda^2 + \chi_3 \Lambda^3 + \chi_4 \Lambda^4 + \chi_5 \Lambda^5. \tag{A.2}$$

In view of (20) and (40), the following identities can be easily verified

$$\begin{bmatrix} \mathbf{A}_1 & \mathbf{A}_2 \\ \mathbf{B}_1 & \mathbf{B}_2 \end{bmatrix} \Lambda^m \begin{bmatrix} -\mathbf{B}_2^{\mathrm{T}} & \mathbf{A}_2^{\mathrm{T}} \\ \mathbf{B}_1^{\mathrm{T}} & -\mathbf{A}_1^{\mathrm{T}} \end{bmatrix} = \mathbf{N}^m, \quad m = 1\text{–}5. \tag{A.3}$$

It follows from (A.2) and (A.3) that

$$\mathbf{P}_k(r/R_k) = \chi_0 \mathbf{I} + \chi_1 \mathbf{N} + \chi_2 \mathbf{N}^2 + \chi_3 \mathbf{N}^3 + \chi_4 \mathbf{N}^4 + \chi_5 \mathbf{N}^5. \tag{A.4}$$

The above expression indicates that the field transfer matrix $\mathbf{P}_k(r/R_k)$ can be determined from the real matrix $\mathbf{N}$, thus the calculation of eigenvectors of (20) can be circumvented.

References

Aboudi, J., 1987. Damage in composites-modelling of imperfect bonding. Compos. Sci. Technol. 28, 103–128.

Achenbach, J.D., Zhu, H., 1990. Effect of interphases on micro and macromechanical behavior of hexagonal-array fiber composites. ASME J. Appl. Mech. 57, 956–963.

Bhaskar, K., Varadan, T.K., 1993. Exact elasticity solution for laminated anisotropic cylindrical shells. ASME J. Appl. Mech. 60, 41–47.

Chen, C.Q., Shen, Y.P., Wang, X.M., 1997. Exact solution of orthotropic cylindrical shell with piezoelectric layers under cylindrical bending. Int. J. Solids Struct. 34, 4481–4491.

Cheng, Z.Q., Kitipornchai, S., 1998. Nonlinear theory for composite laminated shells with interfacial damage. ASME J. Appl. Mech. 65, 711–718.

Cheng, Z.Q., Jemah, A.K., Williams, F.W., 1996. Theory for multilayered anisotropic plates with weakened interfaces. ASME J. Appl. Mech. 63, 1019–1026.

Dvorak, G.J., Zhang, J., 2001. Transformation field analysis of damage evolution in composite materials. J. Mech. Phys. Solids 49, 2517–2541.

Librescu, L., Schmidt, R., 2001. A general linear theory of laminated composite shell featuring interlaminar bonding imperfections. Int. J. Solids Struct. 38, 3355–3375.

Liu, D., Xu, L., Lu, X., 1994. Stress analysis of imperfect composite laminates with an interlaminar bonding theory. Int. J. Numer. Meth. Eng. 37, 2819–2839.

Liu, Y., Ru, C.Q., Schiavone, P., Mioduchowski, A., 2001. New phenomena concerning the effect of imperfect bonding on radial matrix crack in fiber composites. Int. J. Eng. Sci. 39, 2033–2050.

Pan, E., 2001. Exact solution for simply supported and multilayered magneto-electro-elastic plates. ASME J. Appl. Mech. 68, 608–618.

Reddy, J.N., Cheng, Z.Q., 2001. Three-dimensional solutions of smart functionally graded plates. ASME I. Appl. Mech. 68, 234–240.

Ren, J.G., 1987. Exact solutions for laminated cylindrical shells in cylindrical bending. Compos. Sci. Technol. 29, 169–187.

Schmidt, R., Librescu, L., 1999. A general theory of geometrically imperfect laminated composite shells featuring damaged bonding interfaces. Q. J. Mech. Appl. Math. 52, 565–583.

Tarn, J.Q., 2002a. A state space formalism for anisotropic elasticity. Part II: Cylindrical anisotropy. Int. J. Solids Struct. 39, 5157–5172.

Tarn, J.Q., 2002b. Exact solutions of a piezoelectric circular tube or bar under extension, torsion, pressuring, shearing, uniform electric loading and temperature change. Proc. R. Soc. London A 458, 2349–2367.

Tong, J., Nan, C.W., Fu, J., Guan, X., 2001. Effect of inclusion shape on the effective elastic moduli for composites with imperfect interface. Acta Mech. 146, 127–134.

Tullini, N., Savoia, M., Horgan, C.O., 1998. End effect for anti-plane shear deformation of periodically laminated strips with imperfect bonding. J. Elasticity 50, 227–244.

Wang, X., Shen, Y.P., 2002. Two circular inclusions with circumferentially inhomogeneous interfaces interacting with a circular Eshelby inclusion in anti-plane shear. Acta Mech. 158 (1–2), 67–84.

Wang, X.D., Meguid, S.A., 1999. Dynamic interaction between a matrix crack and a circular inhomogeneity with a distinct interface. Int. J. Solids Struct. 36, 517–531.

Yue, Z.Q., Yin, J.H., 1998. Backward transfer-matrix method for elastic analysis of layered solids with imperfect bonding. J. Elasticity 50, 109–128.

Zhong, Z., Meguid, S.A., 1997. On the elastic field of a spherical inhomogeneity with an imperfectly bonded interface. J. Elasticity 46, 91–117.